Transportation on the rotary

2006 J. Phys. A: Math. Gen. 39 14249

(http://iopscience.iop.org/0305-4470/39/46/002)

INSTITUTE OF PHYSICS PUBLISHING JOURNAL OF PHYSICS A: MATHEMATICAL AND GENERAL

J. Phys. A: Math. Gen. **39** (2006) 14249–14261 doi:10.1088/0305-4470/39/46/002

Transportation on the rotary

Ding-wei Huang

Department of Physics, Chung Yuan Christian University, Chung-li, Taiwan

Received 17 February 2006, in final form 7 October 2006
Published 1 November 2006
Online at stacks.iop.org/JPhysA/39/14249

Abstract

We study the mass transportation on a rotary by cellular automata. Various on- and off-ramps are introduced to allow particles to move in and out of the rotary. We obtain the exact results analytically. Distinct phases of the traffic flow are classified completely. Phase diagrams in the full parameter space are derived. We show that the bulk properties and the phase transitions are totally controlled by the operation of ramps. The ramps provide a means to stabilize the density difference on the rotary and thus to support the maximum flow as a distinct phase. The efficiency of transportation can be enhanced by adding more ramps to the rotary. Adding off-ramps is more effective in a low density region, while adding on-ramps is more effective in a high density region. The transition regime between free flow and congestion can be controlled by the order of ramps. When the on-ramps and the off-ramps are located alternately to each other, the intermediate phases are significantly suppressed.

PACS numbers: 89.40.−a, 05.40.−a

1. Introduction

Transportation is an interesting topic and has many applications in modern society [1, 2]. One of the main concerns is to keep the process in the free-flow regime and to avoid the emergence of congestion. Thus, a better understanding of the transition mechanism has always been the focus of research interests. In statistical physics, the phase transition is characterized by the order parameter, which often reflects the bulk property. Conventionally, bulk density is taken as an indicator of the transition, since congestion always appears in a high density region. However, transportation is basically a one-dimensional non-equilibrium process. The phase transition might be better characterized as the boundary-induced [3, 4] instead of the bulk-induced process. Although the ramps only constitute a negligible part of the roadway, various types of complex flow have been observed near the ramps [5–7]. The ramps can be taken as non-trivial boundaries to trigger the phase transitions in bulk. In practice, the ramps become crucial parts to monitor and to control the transitions.

In this work, we study the mass transportation on a rotary. Traffic conditions are fully controlled by the operation of ramps [8]. We are able to obtain the exact phase diagrams

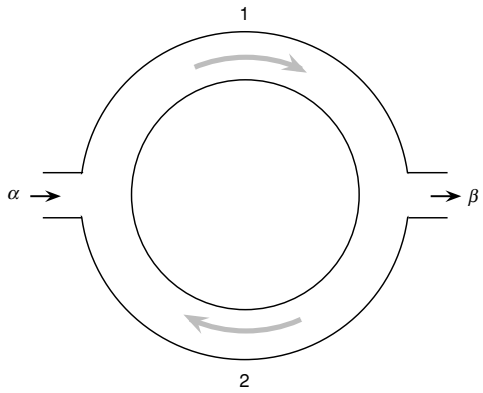

Figure 1. System configuration of a traffic rotary with two ramps. The particles move clockwise as shown by the grey arrows. The upper and lower branches are labelled as section 1 and section 2, respectively.

analytically. All the distinct phases in a full parameter space can be classified completely. The model will be introduced in the following section. Two issues will be addressed separately. Section 3 presents the discussions on the number of ramps. The order of ramps will be discussed in section 4.

2. Model

Instead of continuous differential equations, the dynamics is prescribed by cellular automata. Both space and time are discretized. The rotary is taken as a one-dimensional circular lattice. Each site can be accommodated by one particle only. At each time step, a particle hops forward to the next site provided it is empty in the previous time step. This update rule is applied to all particles synchronously, which is known as a parallel-update scheme and provides much stronger correlation than the conventional sequential-update scheme does. As the movement is along one direction only, the dynamics is also known as an asymmetric simple exclusion process (ASEP) [9, 10]. The number of particles on the rotary is not a conserved quantity. Particles are allowed to move in and out of the rotary through the ramps. Each ramp is a predestinated site operated by a stochastic rate. At the on-ramp, a new particle will be injected with a probability α when the site is empty; at the off-ramp, when the site is occupied, the particle will be removed with a probability β. These rates are the control parameters of the system.

For a simple configuration shown in figure 1, the rotary can be effectively divided into two homogeneous sections labelled by 1 and 2. The operation of the on-ramp α can be replaced by an effective injection α' for section 1 and an effective removal β' for section 2, and the off-ramp β by an effective removal β'' for section 1 and an effective injection α'' for section 2. The traffic conditions can then be specified in section 1 by α' and β'' and in section 2 by α'' and β'. These effective rates can be obtained by a self-consistent mean-field theory [8]. In the free flow, the traffic is controlled by the injection, i.e.

$$\rho_1 = j_1 = \frac{\alpha'}{1+\alpha'}, \qquad \rho_2 = j_2 = \frac{\alpha''}{1+\alpha''}, \tag{1}$$

where ρ and j denote bulk density and flow, respectively, within each section, which is indicated by the subscript. The flow conservation across the on-ramp and off-ramp gives the

following equations:

$$j_2 + (1-\rho_1)\alpha = j_1, \qquad j_1 - \rho_1\beta = j_2. \tag{2}$$

It is interesting to note that the local densities at the on-ramp and off-ramp assume the same value as the bulk density in section 1. These equations can also be expressed as

$$\frac{\alpha''}{1+\alpha''} + \frac{1}{1+\alpha'}\alpha = \frac{\alpha'}{1+\alpha'}, \qquad \frac{\alpha'}{1+\alpha'} - \frac{\alpha'}{1+\alpha'}\beta = \frac{\alpha''}{1+\alpha''}. \tag{3}$$

Together, the effective injection can be solved,

$$\alpha' = \frac{\alpha}{\beta}, \qquad \alpha'' = \frac{\alpha(1-\beta)}{\beta(1+\alpha)}. \tag{4}$$

For asymmetric simple exclusion processes in the free-flow regime, the bulk properties are determined by the injection boundary. The local density at the removal boundary might be different from the bulk value. The self-consistence at the effective removal boundary gives the following equations:

$$\rho_1\beta' = j_2, \qquad \rho_1\beta'' = j_1. \tag{5}$$

These equations can be expressed as

$$\frac{\alpha'}{1+\alpha'}\beta' = \frac{\alpha''}{1+\alpha''}, \qquad \frac{\alpha'}{1+\alpha'}\beta'' = \frac{\alpha'}{1+\alpha'}. \tag{6}$$

The effective removal can then be solved,

$$\beta' = 1-\beta, \qquad \beta'' = 1. \tag{7}$$

To ensure the free-flow conditions, the constraints $\alpha' < \beta''$ and $\alpha'' < \beta'$ have to be imposed. It is easy to see that the free flow in section 1 provides the crucial constraint $\alpha < \beta$ for free flow on the rotary.

In the congestion, the traffic is controlled by the removal, i.e.

$$\rho_1 = 1 - j_1 = \frac{1}{1+\beta''}, \qquad \rho_2 = 1 - j_2 = \frac{1}{1+\beta'}. \tag{8}$$

The flow conservation gives the following equations:

$$\frac{\beta'}{1+\beta'} + \frac{\beta''}{1+\beta''}\alpha = \frac{\beta''}{1+\beta''}, \qquad \frac{\beta''}{1+\beta''} - \frac{1}{1+\beta''}\beta = \frac{\beta'}{1+\beta'}. \tag{9}$$

The effective removal can be solved,

$$\beta' = \frac{\beta(1-\alpha)}{\alpha(1+\beta)}, \qquad \beta'' = \frac{\beta}{\alpha}. \tag{10}$$

The self-consistence at the effective injection boundary gives the following equations:

$$\frac{\beta''}{1+\beta''}\alpha' = \frac{\beta''}{1+\beta''}, \qquad \frac{\beta''}{1+\beta''}\alpha'' = \frac{\beta'}{1+\beta'}. \tag{11}$$

The effective injection can then be solved,

$$\alpha' = 1, \qquad \alpha'' = 1-\alpha. \tag{12}$$

To ensure the congestion conditions, the constraints $\alpha' > \beta''$ and $\alpha'' > \beta'$ have to be imposed. Again, the congestion in section 1 provides the crucial constraint $\alpha > \beta$ for congestion on the rotary.

On a homogeneous roadway, the traffic conditions can be categorized into free flow (F) and jam (J). With a naive combination, the two sections could provide four distinct phases. However, only two of them can be realized. When the injection α is less than the removal β,

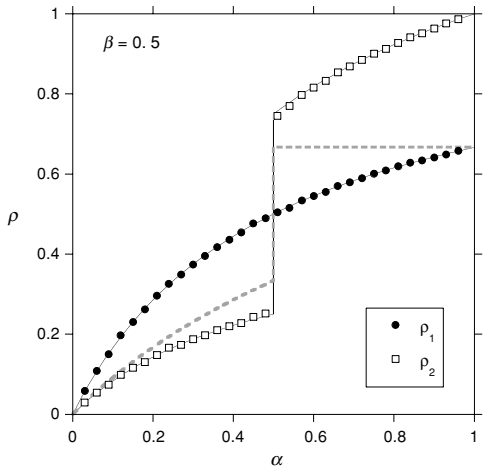

Figure 2. α dependence of the bulk densities at $\beta = 0.5$. The numerical simulations can be correctly reproduced by the analytical results, which are shown by the solid lines. The results for a simple roadway are shown by the grey dashed line. The numerical data are obtained by simulations on a rotary of 2000 sites, with each branch consisting of 1000 sites. As the bulk densities are plotted separately for each branch, the results are independent of both the rotary size and the ratio between the two branches.

free flow can be maintained in both sections; when the injection α is larger than the removal β, both sections become congested. It is impossible to have one section congested while the other free of jams. The typical bulk densities ρ_1 and ρ_2 for these two sections are shown in figure 2. The analytical expressions can be summarized as follows:

$$\text{(FF)} \quad \rho_1 = \frac{\alpha}{\alpha + \beta}, \qquad \rho_2 = \rho_1(1 - \beta); \tag{13}$$

$$\text{(JJ)} \quad \rho_1 = \frac{\alpha}{\alpha + \beta}, \qquad \rho_2 = \rho_1(1 + \beta). \tag{14}$$

As α and β vary, ρ_1 changes continuously, while ρ_2 displaces an abrupt transition at $\alpha = \beta$. It is interesting to note that the phase diagram is the same as in the case of a simple straight roadway, i.e. $\alpha < \beta$ for free flow and $\alpha > \beta$ for congestion. However, the α dependence of the density is quite different. The comparison is also shown in figure 2. For a straight roadway, the density saturates after the transition, i.e. the density becomes independent of α in the jam phase. (In the free-flow phase, the density is independent of β.) For a straight roadway, the density depends only on one of the two control parameters. With the rotary, the density depends on both α and β. Thus, in the jam phase shown in figure 2, both ρ_1 and ρ_2 continue to rise as α further increases.

3. Number of ramps

Now we consider the effect of adding one more ramp. With one more off-ramp, the configuration is shown in the inset of figure 4. The analytical results can be derived similarly as in the previous section (see the appendix). To compare with the basic two-ramp model shown in figure 1, we assume that the two off-ramps are operated at the same rate, which is simply taken as $\beta/2$ to have the total rate fixed at β. As the rotary is now divided into three sections, the naive combination would predict eight possible phases. In fact, only the

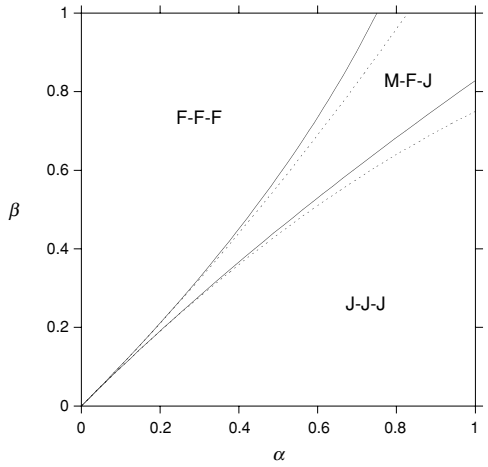

Figure 3. Phase diagram for a rotary with three ramps. The solid lines show the results for one on-ramp and two off-ramps (inset of figure 4). The dotted lines show the results for two on-ramps and one off-ramp (inset of figure 5).

following three distinct phases can be realized:

$$\text{(FFF)} \quad \alpha < \beta - \tfrac{1}{4}\beta^2, \tag{15}$$

$$\text{(MFJ)} \quad \beta - \tfrac{1}{4}\beta^2 < \alpha < \beta + \tfrac{1}{4}\beta^2, \tag{16}$$

$$\text{(JJJ)} \quad \alpha > \beta + \tfrac{1}{4}\beta^2. \tag{17}$$

Besides free flow (F) and jam (J), the maximum flow (M) is observed as a new phase. The phase diagram is shown in figure 3. Basically, when the injection is small (and the removal is large), the free flow can be maintained in all the three sections; when the injection is large (and the removal is small), all the three sections are congested. The transition between these two conventional phases can still be observed as along the line $\alpha = \beta$. The newly added off-ramp provides a mean to stabilize the occurrence of maximum flow. The transition boundary is extended into a distinct phase (MFJ), where section 1 is saturated to the maximum flow, free flow is maintained in section 2 and traffic jams dominate in section 3. Such effects are most prominent when both α and β are large. The results of bulk densities are shown in figure 4. As the maximum flow can only be stabilized in section 1, ρ_1 changes continuously, while both ρ_2 and ρ_3 displace abrupt transitions. In the low density free flow, we have $\rho_1 > \rho_2 > \rho_3$, while in the high density congestion, we have $\rho_1 < \rho_2 < \rho_3$. The transition of ρ_3 appears at a smaller α; the transition of ρ_2 appears at a larger α. In between these two transitions, ρ_1 is fixed at the maximum flow. The analytical expressions for the above results can also be obtained as follows:

$$\text{(FFF)} \quad \rho_1 = \frac{\alpha}{\alpha + \beta - \frac{\beta^2}{4}}, \qquad \rho_2 = \rho_1\left(1 - \frac{\beta}{2}\right), \qquad \rho_3 = \rho_1\left(1 - \frac{\beta}{2}\right)^2; \tag{18}$$

$$\text{(MFJ)} \quad \rho_1 = \frac{1}{2}, \qquad \rho_2 = \rho_1\left(1 - \frac{\beta}{2}\right), \qquad \rho_3 = \rho_1(1 + \alpha); \tag{19}$$

$$\text{(JJJ)} \quad \rho_1 = \frac{\alpha}{\alpha + \beta + \frac{\beta^2}{4}}, \qquad \rho_2 = \rho_1\left(1 + \frac{\beta}{2}\right), \qquad \rho_3 = \rho_1\left(1 + \frac{\beta}{2}\right)^2. \tag{20}$$

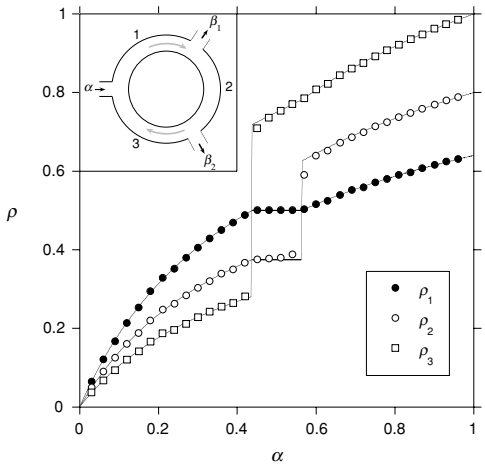

Figure 4. α dependence of the bulk densities on a rotary with one on-ramp (α) and two off-ramps (β_1, β_2). The system configuration is shown in the inset. The rotary is divided into three parts labelled by the number. To compare with figure 2, we assume $\beta_1 = \beta_2 = \beta/2 = 0.25$. The analytical results are shown by the solid lines, which reproduce the data correctly. Again, the numerical data are independent of the length scales.

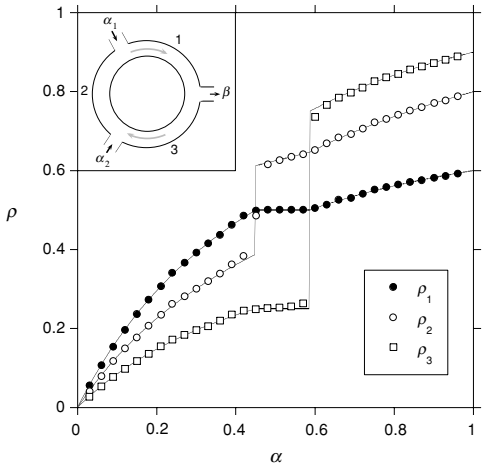

Figure 5. α dependence of the bulk densities on a rotary with two on-ramps (α_1, α_2) and one off-ramp (β). The system configuration is shown in the inset. In contrast to figure 4, the number indexes 1, 2, 3 are now labelled against the traffic direction. We assume $\alpha_1 = \alpha_2 = \alpha/2$ and $\beta = 0.5$. The analytical results are shown by the solid lines, which reproduce the data correctly.

In contrast, if an on-ramp is added, the configuration is shown in the inset of figure 5, where the two on-ramps are operated at the same rate of $\alpha/2$ to have the total rate fixed at α. The same three phases can be observed with a slight shift in the boundary, see figure 3. The analytical results can be expressed as follows:

$$\text{(FFF)} \quad \beta > \alpha + \tfrac{1}{4}\alpha^2, \tag{21}$$

$$\text{(MJF)} \quad \alpha - \tfrac{1}{4}\alpha^2 < \beta < \alpha + \tfrac{1}{4}\alpha^2, \tag{22}$$

$$\text{(JJJ)} \quad \beta < \alpha - \tfrac{1}{4}\alpha^2. \tag{23}$$

We note that if the index is relabelled as along the traffic direction, the middle phase will become (MFJ) again. It is interesting to observe that these two cases can be mapped into each other by the time reversal symmetry: $\alpha \leftrightarrow \beta$, $\rho \leftrightarrow (1-\rho)$, F (free) $\leftrightarrow$ J (jam). The results of bulk densities are shown in figure 5. The analytical results can also be obtained as follows:

$$\begin{aligned}
\text{(FFF)}\quad & \rho_1 = 1 - \frac{\beta}{\beta + \alpha + \frac{\alpha^2}{4}}, \\
& \rho_2 = 1 - (1-\rho_1)\left(1 + \frac{\alpha}{2}\right), \\
& \rho_3 = 1 - (1-\rho_1)\left(1 + \frac{\alpha}{2}\right)^2;
\end{aligned} \tag{24}$$

$$\begin{aligned}
\text{(MJF)}\quad & \rho_1 = \frac{1}{2}, \\
& \rho_2 = \rho_1\left(1 + \frac{\alpha}{2}\right), \\
& \rho_3 = \rho_1(1-\beta);
\end{aligned} \tag{25}$$

$$\begin{aligned}
\text{(JJJ)}\quad & \rho_1 = 1 - \frac{\beta}{\beta + \alpha - \frac{\alpha^2}{4}}, \\
& \rho_2 = 1 - (1-\rho_1)\left(1 - \frac{\alpha}{2}\right), \\
& \rho_3 = 1 - (1-\rho_1)\left(1 - \frac{\alpha}{2}\right)^2.
\end{aligned} \tag{26}$$

The above expressions have been manipulated to show the symmetry explicitly. For both cases, the maximum flow emerges between an on-ramp and an off-ramp. The on-ramp is located before the off-ramp along the traffic direction. As α increases, the abrupt transition moves against the traffic direction, i.e. it first emerges in the upstream of the maximum flow and then propagates against the traffic direction to the downstream of the maximum flow.

Theoretically, we can compare figure 4 and figure 5 quantitatively at fixed α and β. Higher densities are found in the former. Compared to adding one on-ramp to the basic configuration shown in figure 1, adding one off-ramp results in higher densities in both low density regime and high density regime. In the low density free flow, higher density implies higher flow, while in the high density congestion, higher density results in lower flow. In such comparisons, the total rate is fixed. When two ramps of the same kind are involved, the total rate is equally shared by the two ramps.

4. Order of ramps

Next, we consider the rotary with four ramps shown in the inset of figure 7. In this configuration, the maximum flow can only be observed in section 1. As the congestion developed, the traffic jams first emerge in section 4. Then the jams appear in section 3, as against the traffic direction. Finally, the traffic jams emerge in section 2 just before the entire rotary becomes congested. In total, there are four distinct phases as follows:

$$\text{(FFFF)}\quad \alpha + \tfrac{1}{4}\alpha^2 < \beta - \tfrac{1}{4}\beta^2, \tag{27}$$

$$\text{(MFFJ)}\quad \alpha - \tfrac{1}{4}\alpha^2 < \beta - \tfrac{1}{4}\beta^2 < \alpha + \tfrac{1}{4}\alpha^2, \tag{28}$$

$$\text{(MFJJ)}\quad \beta - \tfrac{1}{4}\beta^2 < \alpha - \tfrac{1}{4}\alpha^2 < \beta + \tfrac{1}{4}\beta^2, \tag{29}$$

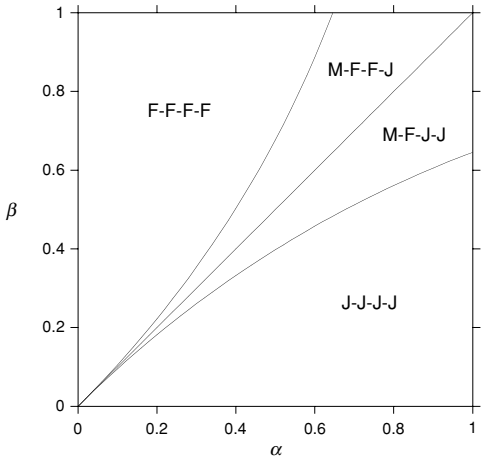

Figure 6. Phase diagram for a rotary with four ramps (inset of figure 7).

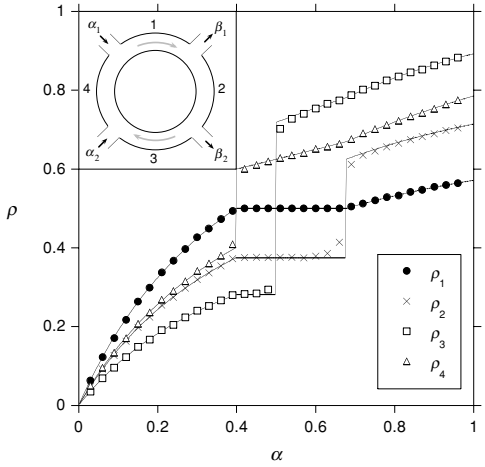

Figure 7. α dependence of the bulk densities on a rotary with four ramps. The system configuration is shown in the inset. We assume $\alpha_1 = \alpha_2 = \alpha/2$ and $\beta_1 = \beta_2 = \beta/2$. Again, the numerical data can be exactly reproduced by the analytical results.

$$\text{(JJJJ)} \quad \beta + \tfrac{1}{4}\beta^2 < \alpha - \tfrac{1}{4}\alpha^2. \tag{30}$$

The phase diagram is shown in figure 6. Two intermediate phases develop in between the transition from free flow (FFFF) to the congestion (JJJJ). With section 1 saturated to maximum flow, section 2 (downstream) must be free of jams and section 4 (upstream) must be congested. The traffic in section 3 can be either free or jammed, which results in two intermediate phases. The onset of the transitions is signified by the saturation in section 1. As α increases, the congestion emerges from the upstream and moves against the traffic direction to the downstream. The bulk densities are shown in figure 7. Again, the density in section 1 changes continuously, while abrupt transitions appear in the other three sections. In the free-flow regime, section 1 has the highest density; in the congestion regime, the density in section 1 becomes the lowest one.

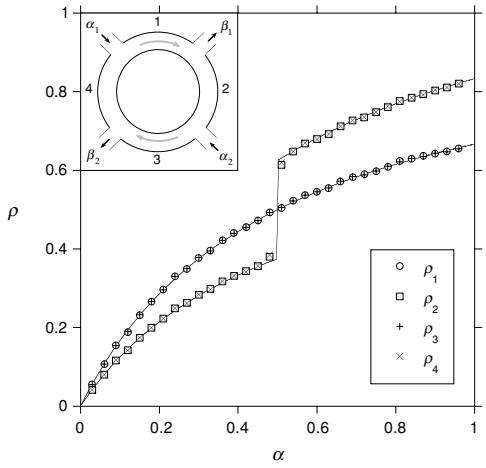

Figure 8. Compared to figure 7, the locations of α_2 and β_2 are switched. The intermediate phases disappear.

The four-ramp rotary can have a different topology, as shown in the inset of figure 8. Compared to figure 7, the order of ramps has been rearranged. The on-ramps and off-ramps are now distributed alternately along the rotary. By symmetry, section 1 is equivalent to section 3, and section 2 is equivalent to section 4. It is interesting to observe that, when assuming $\alpha_1 = \alpha_2 = \alpha/2$ and $\beta_1 = \beta_2 = \beta/2$, there are only two distinct phases as follows:

$$\text{(FFFF)} \quad \alpha < \beta, \tag{31}$$

$$\text{(JJJJ)} \quad \alpha > \beta. \tag{32}$$

The four sections can only be all congested or all freed of jams. There are no intermediate phases. As expected, the densities in sections 1 and 3 change continuously; the densities in sections 2 and 4 show an abrupt jump at $\alpha = \beta$, see figure 8.

5. Discussions

In this paper, we study the mass transportation on a rotary. Traffic conditions are fully controlled by the operation of ramps, which can be taken as non-trivial boundaries to trigger the phase transitions in bulk. We are able to obtain the exact phase diagram analytically. The distinct phases in a full parameter space can be classified completely. With a simple model, we show that the situations in between any two consecutive ramps can be categorized into free flow, congestion and maximum flow. However, not all the combinations can be realized on the rotary. Along the traffic direction, the free flow will not follow the congestion directly. When both free flow and congestion coexist on the rotary, there must involve a section of maximum flow in the middle. The section of maximum flow must be started at the on-ramp and ended at the off-ramp.

As we focus on the bulk properties, the phase diagram provides a convenient tool to classify the distinct traffic states. Along the phase boundaries, coexistent phases can be expected. For example, along the boundary between (FFF) and (MFJ) in figure 3, a conventional domain well can be observed in section 3 of the rotary. The free flow can be sustained near the junction connected to section 2, while the congestion persists near the junction connected to

section 1. Similarly, along the boundary between (MFJ) and (JJJ) in figure 3, a domain well can be observed in section 2. It is interesting to note that the domain well will not appear in section 1, where the maximum flow emerges. In this simple model, the density profile is flat except along the phase boundary and/or near the ramps. We show that the bulk density can be obtained by the mean-field theory, which is also confirmed by numerical simulations. To obtain the non-flat distribution near the ramps, more elaborate methods have to be resorted. As the ramp consists of a single site on the lattice, the system can be decoupled into homogeneous subsystems. The effective rates for each homogeneous section can be uniquely determined. The local density at the ramp is also correctly prescribed. Thus, we would expect that the matrix product ansatz developed in the homogeneous system can be applied to give a detailed density profile on the rotary.

In the conventional boundary-induced phase transitions, i.e. along a simple roadway with two open ends, the bulk properties depend only on one of the two boundaries. In the phase of free flow, the traffic flow is controlled by the injection boundary and can be written as $\alpha/(1+\alpha)$. In the phase of congestion, the traffic flow is then controlled by the removal boundary and can be written as $\beta/(1+\beta)$. Thus, tuning the removal boundary in the low density regime will only result in a slight change in the boundary layer. Similarly, tuning the injection boundary in the high density regime will have no effects on the bulk properties. With a rotary, in contrast, the traffic flow for effective transportation from an on-ramp to off-ramp depends on both boundaries and can be written as $\alpha\beta/(\alpha+\beta)$. The same expression can be applied to both free flow and congestion. As can be expected, the efficiency of transportation is reduced. At the off-ramp, not all the particles will be removed. With a finite probability $(1-\beta)$, a particle might be left on the rotary. However, the traffic flow can now be controlled by both α and β. The dependence on both parameters could provide more flexibility to implant the control scheme and to monitor the traffic conditions.

With fixed total injection α and total removal β, the efficiency of transportation can be enhanced by adding more ramps to the rotary, either on-ramps or off-ramps. In the low density region, the increase of efficiency can be observed as the increase of bulk density, while in the high density region, the increase of efficiency results in a decrease of bulk density. We observed that adding one off-ramp always results in a higher bulk density than adding one on-ramp does. To have a reasonable comparison, the operation rates of the ramps should be properly rescaled. With N on-ramps and M off-ramps, the injection rate at each on-ramp is α/N and the removal rate at each off-ramp is β/M. Thus, the total rates are fixed and shared equally. We then have the conclusion that adding an off-ramp is more effective in a low density region, while adding an on-ramp is more effective in a high density region. In the case of N on-ramps and M off-ramps, the free flow can be maintained in the entire rotary in the regime:

$$\left(1+\frac{\alpha}{N}\right)^N - 1 < 1 - \left(1-\frac{\beta}{M}\right)^M. \tag{33}$$

On the other end, the entire rotary is congested in the regime:

$$1 - \left(1-\frac{\alpha}{N}\right)^N > \left(1+\frac{\beta}{M}\right)^M - 1. \tag{34}$$

In between these two phases, there are $(N+M-2)$ intermediate phases along the strip $\alpha \sim \beta$. The special cases of section 3 can be reproduced as $(N=1, M=2)$ and $(N=2, M=1)$.

As the efficiency is mainly controlled by the number of ramps, the order of ramps has a great influence on the intermediate phases in the transition. Basically, there are two different kinds of arrangement. In the first kind, the on-ramps are near to each other and located on one side of the rotary, while the off-ramps are on the other side. Then the maximum flow can

only be supported in a single section of the rotary. The free flow and the congestion are well separated by various intermediate phases. In the second kind, the on-ramps and off-ramps are located alternately to each other. The maximum flow can be supported in multiple sections of the rotary. When the injection rate α is spread uniformly among the on-ramps and the removal rate β among the off-ramps, the intermediate phases are significantly suppressed. In figure 8, all the intermediate phases disappear. These are only two distinct phases: (FFFF) and (JJJJ). If this constraint is removed, i.e. the four ramps are specified independently by $\alpha_1, \alpha_2, \beta_1, \beta_2$, there are six distinct phases as follows:

$$\text{(FFFF)} \quad A_1 - B_2 < \min[2\alpha_1\beta_1, 2\alpha_2\beta_2], \tag{35}$$

$$\text{(JJJJ)} \quad B_1 - A_2 < \min[2\alpha_1\beta_1, 2\alpha_2\beta_2], \tag{36}$$

$$\text{(MFFJ)} \quad B_2 + 2\alpha_2\beta_2 < A_1 < B_1, \tag{37}$$

$$\text{(MFJJ)} \quad A_2 + 2\alpha_2\beta_2 < B_1 < A_1, \tag{38}$$

$$\text{(FJMF)} \quad B_2 + 2\alpha_1\beta_1 < A_1 < B_1, \tag{39}$$

$$\text{(JJMF)} \quad A_2 + 2\alpha_1\beta_1 < B_1 < A_1, \tag{40}$$

where $A_1 \equiv (\alpha_1 + \alpha_2 + \alpha_1\alpha_2)$, $A_2 \equiv (\alpha_1 + \alpha_2 - \alpha_1\alpha_2)$, $B_1 \equiv (\beta_1 + \beta_2 + \beta_1\beta_2)$ and $B_2 \equiv (\beta_1 + \beta_2 - \beta_1\beta_2)$. In contrast, for the first kind of arrangement shown in figure 7, the number of distinct phases remains at four:

$$\text{(FFFF)} \quad A_1 - B_2 < 0, \tag{41}$$

$$\text{(JJJJ)} \quad B_1 - A_2 < 0, \tag{42}$$

$$\text{(MFFJ)} \quad A_2 < B_2 < A_1, \tag{43}$$

$$\text{(MFJJ)} \quad B_2 < A_2 < B_1. \tag{44}$$

As the number of ramps further increases, the results can be easily extended.

Appendix

For the configuration shown in the inset of figure 4, the rotary can be effectively divided into three homogeneous sections labelled by 1, 2 and 3. The operation of α, β_1 and β_2 can be replaced by effective rates (α', β'), (α'', β'') and (α''', β'''), respectively. The traffic conditions can then be specified by (α', β'') in section 1, (α'', β''') in section 2 and (α''', β') in section 3. In the free flow, the traffic is controlled by the injection as

$$\rho_1 = \frac{\alpha'}{1+\alpha'}, \qquad \rho_2 = \frac{\alpha''}{1+\alpha''}, \qquad \rho_3 = \frac{\alpha'''}{1+\alpha'''}. \tag{A.1}$$

The flow conservation across the ramps gives the following equations:

$$\begin{aligned} &\frac{\alpha'''}{1+\alpha'''} + \frac{1}{1+\alpha'}\alpha = \frac{\alpha'}{1+\alpha'}, \\ &\frac{\alpha'}{1+\alpha'} - \frac{\alpha'}{1+\alpha'}\beta_1 = \frac{\alpha''}{1+\alpha''}, \\ &\frac{\alpha''}{1+\alpha''} - \frac{\alpha''}{1+\alpha''}\beta_2 = \frac{\alpha'''}{1+\alpha'''}. \end{aligned} \tag{A.2}$$

The analytical expressions for the effective injection can be obtained:

$$\begin{aligned}\alpha' &= \frac{\alpha}{\beta_1+\beta_2-\beta_1\beta_2},\\ \alpha'' &= \frac{\alpha(1-\beta_1)}{\beta_1+\beta_2-\beta_1\beta_2+\alpha\beta_1},\\ \alpha''' &= \frac{\alpha(1-\beta_1)(1-\beta_2)}{(1+\alpha)(\beta_1+\beta_2-\beta_1\beta_2)}.\end{aligned} \tag{A.3}$$

The self-consistence at the effective removal boundary gives the following equations:

$$\frac{\alpha'}{1+\alpha'}\beta' = \frac{\alpha'''}{1+\alpha'''}, \qquad \frac{\alpha'}{1+\alpha'}\beta'' = \frac{\alpha'}{1+\alpha'}, \qquad \frac{\alpha''}{1+\alpha''}\beta''' = \frac{\alpha''}{1+\alpha''}. \tag{A.4}$$

The analytical expressions for the effective removal can then be obtained:

$$\beta' = (1-\beta_1)(1-\beta_2), \qquad \beta'' = 1, \qquad \beta''' = 1. \tag{A.5}$$

The free-flow conditions impose the constraints $\alpha' < \beta''$, $\alpha'' < \beta'''$ and $\alpha''' < \beta'$. It can be shown that the free flow in section 1 provides the crucial constraint $\alpha < (\beta_1+\beta_2-\beta_1\beta_2)$ for free flow on the rotary.

Similarly, the traffic in the congestion is controlled by the removal as

$$\rho_1 = \frac{1}{1+\beta''}, \qquad \rho_2 = \frac{1}{1+\beta'''}, \qquad \rho_3 = \frac{1}{1+\beta'}. \tag{A.6}$$

The flow conservation gives the following equations:

$$\begin{aligned}\frac{\beta'}{1+\beta'} + \frac{\beta''}{1+\beta''}\alpha &= \frac{\beta''}{1+\beta''},\\ \frac{\beta''}{1+\beta''} - \frac{1}{1+\beta''}\beta_1 &= \frac{\beta'''}{1+\beta'''},\\ \frac{\beta'''}{1+\beta'''} - \frac{1}{1+\beta'''}\beta_2 &= \frac{\beta'}{1+\beta'}.\end{aligned} \tag{A.7}$$

The effective removal can be solved,

$$\begin{aligned}\beta' &= \frac{(1-\alpha)(\beta_1+\beta_2+\beta_1\beta_2)}{\alpha(1+\beta_1)(1+\beta_2)},\\ \beta'' &= \frac{\beta_1+\beta_2+\beta_1\beta_2}{\alpha},\\ \beta''' &= \frac{\beta_1+\beta_2+\beta_1\beta_2-\alpha\beta_1}{\alpha(1+\beta_1)}.\end{aligned} \tag{A.8}$$

The self-consistence at the effective injection boundary gives the following equations:

$$\frac{\beta''}{1+\beta''}\alpha' = \frac{\beta''}{1+\beta''}, \qquad \frac{\beta''}{1+\beta''}\alpha'' = \frac{\beta'''}{1+\beta'''}, \qquad \frac{\beta'''}{1+\beta'''}\alpha''' = \frac{\beta'}{1+\beta'}. \tag{A.9}$$

The effective injection can then be solved,

$$\alpha' = 1, \qquad \alpha'' = \frac{\beta_1+\beta_2+\beta_1\beta_2-\alpha\beta_1}{\beta_1+\beta_2+\beta_1\beta_2}, \qquad \alpha''' = \frac{(1-\alpha)(\beta_1+\beta_2+\beta_1\beta_2)}{\beta_1+\beta_2+\beta_1\beta_2-\alpha\beta_1}. \tag{A.10}$$

The congestion conditions impose the constraints $\alpha' > \beta''$, $\alpha'' > \beta'''$ and $\alpha''' > \beta'$. Again, the congestion in section 1 provides the crucial constraint $\alpha > (\beta_1+\beta_2+\beta_1\beta_2)$ for congestion on the rotary.

In the transition region in between free flow and congestion, i.e. $(\beta_1 + \beta_2 - \beta_1\beta_2) < \alpha < (\beta_1 + \beta_2 + \beta_1\beta_2)$, these effective rates can also be obtained by the self-consistent mean-field approach as

$$\alpha' = 1, \qquad \alpha'' = \frac{1-\beta_1}{1+\beta_1}, \qquad \alpha''' = \frac{\beta_2(1-\alpha)}{\beta_1 + 2\beta_2 - \alpha}, \tag{A.11}$$

$$\beta' = \frac{1-\alpha}{1+\alpha}, \qquad \beta'' = 1, \qquad \beta''' = \frac{\beta_2(1-\beta_1)}{\alpha - \beta_1}. \tag{A.12}$$

The traffic conditions on the rotary can be specified as $\alpha' = \beta'' = 1$, $\alpha'' < \beta'''$ and $\alpha''' > \beta'$, i.e. the (MFJ) phase. The bulk densities have the following simple expressions:

$$\rho_1 = \tfrac{1}{2}, \qquad \rho_2 = \tfrac{1}{2}(1-\beta_1), \qquad \rho_3 = \tfrac{1}{2}(1+\alpha). \tag{A.13}$$

The analytical results for other rotaries can also be derived by similar approaches.

References

[1] Chowdhury D, Santen L and Schadschneider A 2000 *Phys. Rep.* **329** 199
[2] Mahnke R, Kaupužs J and Lubashevsky I 2005 *Phys. Rep.* **408** 1
[3] Krug J 1991 *Phys. Rev. Lett.* **67** 1882
[4] Appert C and Santen L 2001 *Phys. Rev. Lett.* **86** 2498
[5] Kerner B S and Rehborn H 1997 *Phys. Rev. Lett.* **79** 4030
[6] Helbing D and Treiber M 1998 *Phys. Rev. Lett.* **81** 3042
[7] Lee H Y, Lee H W and Kim D 1998 *Phys. Rev. Lett.* **81** 1130
[8] Huang D W 2005 *Phys. Rev.* **72** 016102
[9] Derrida B and Evans M R 1997 *Nonequilibrium Statistical Mechanics in One Dimension* ed V Privman (Cambridge: Cambridge University Press)
[10] Derrida B 1998 *Phys. Rep.* **301** 65